Electronic Supplementary Material (ESI) for Physical Chemistry Chemical Physics.
This journal is © the Owner Societies 2017

Supplementary Information for:

Revealing Vilazodone's Binding Mechanism Underlying Its Partial Agonism to 5-HT_{1A} Receptor in the Treatment of Major Depressive Disorder

Guoxun Zheng[a, b], Weiwei Xue[a, *], Fengyuan Yang[a, b], Yang Zhang[a, b], Yuzong Chen[c], Xiaojun Yao[d] and Feng Zhu[a, b, *]

[a] Innovative Drug Research and Bioinformatics Group, School of Pharmaceutical Sciences and Collaborative Innovation Center for Brain Science, Chongqing University, Chongqing 401331, China

[b] Innovative Drug Research and Bioinformatics Group, College of Pharmaceutical Sciences, Zhejiang University, Hangzhou, Zhejiang 310058, China

[c] Bioinformatics and Drug Design Group, Department of Pharmacy, National University of Singapore, Singapore 117543, Singapore

[d] State Key Laboratory of Applied Organic Chemistry and Department of Chemistry, Lanzhou University, Lanzhou 730000, China

*Corresponding Authors:

Prof. Feng Zhu (zhufeng.ns@gmail.com; zhufeng@zju.edu.cn); A/Prof. Weiwei Xue (xueww@cqu.edu.cn)

Supporting Information

Detailed Process for Homology Model

The 5-HT_{1A} receptor was a 7-transmembrane protein consist of 422 residues in total. Among them, amino acid sequence with the 284 residues (V33 to K232, K264 to A274, and V344 to K416) of human 5-HT_{1A} receptor was aligned with that of the template of crystal structure of β_2AR (E30 to C341) with the 312 residues using *ClustalX 2.0*[1] and then visualized by *ESPript 3.0*[2]. The amino acid sequence (K264 to A274) taken from the intracellular region was used to construct the intracellular loop, where there was no crystal structural information on the template. The homology model of 5-HT_{1A}R was carried out by using the automated mode of *SWISS-MODEL* server[3] on the template of the crystal structure of β_2AR. It was noted that the 284 residues but not the 422 residues were used to construct the human 5-HT_{1A}R model based on the template. The other 138 residues were removed for the following reasons:

Firstly, the 284 residues covered the 7-transmembrane region (TM1-7) after the initial sequence alignment of the target and template where there were 312 residues (E30 to C341) structural information on the template of crystal structure of β_2AR. However, the other 138 residues located in the loop region and there was no structural information available in this region on the template. Secondly, this loop region was built via *ab initio* method due to the lack of structural information in this region on the template by using the automated mode of *SWISS-MODEL* server[3]. The *ab initio* homology model method was not appropriate to predict the loop region with too many residues (138)[4,5], because this may lead to larger errors for results. Thirdly, the 138 residues were located far away from the binding pocket and they had little effects on ligands binding to the binding pocket, which was the focus of this work. In sum, the redundant residues in the loop region were removed and the sequence with 11 residues (K264 to A274) were taken from this region to build the loop. Meanwhile, the similar method has been conducted in other related researches[6,7].

Detailed Protocol for Molecular Docking

First, the initial docking poses of 51 ligands to 5-HT_{1A} receptor were performed using *Glide software*[8] implemented in Schrödinger suite of software (Maestro 9.3) with the default settings of standard precision mode. The 3D structures of 51 ligands were obtained via *ChemBioOffice 14*. After that, the structures of 51 ligands were preprocessed by *LigPrep* with *OPLS_2005* force field and the conformations with low energy were obtained. The ionized state was assigned by *Epik* at pH value of 7.0±2.0. Second, the ligand P0G from the co-crystal structure (PDB ID:3SN6) was introduced to the modelled 5-HT_{1A} receptor by *PyMOL's align* operation[9]. Then, the protein was preprocessed via *Protein Preparation Wizard* in *Maestro* to add hydrogen atoms, assign partial charges using *OPLS_2005* force field. The minimization was terminated until the RMSD reached the maximum value of 0.30 Å. Third, the docking grid box was centered on P0G in 5-HT_{1A} receptor by *Receptor Grid Generation* tool in *Glide*[8]. In molecular docking, the protein was rigid and the ligands were flexible. In particular, 5,000 poses were generated in the initial stage of docking, among which

400 poses were selected for energy minimization by 100 steps of conjugate gradient minimization.

Detailed Protocol for MD Simulation

Prior to MD simulation, all systems were subjected to initial energy minimization to remove energetically unfavorable contacts by two steps. The first energy minimization step was to apply harmonic restraints on lipid and solute atoms (force constant $= 10.0\ \mathrm{kcal/mol/Å^2}$) and then to release all atoms to move freely for second step. In each step, full systems were minimized for 10,000 steps, of which the first 5,000 steps used the steepest descent method and the remaining steps used the conjugate gradient method. After that, the whole system was gradually heated from 0 to 310K in the NVT ensemble with the receptor and ligand restrained through two sequential stages over a period of 100ps. Firstly, systems were heated to 100K and gradually heated to 310K. Subsequently, 10 times unconstrained equilibration (5ns) at the temperature of 310K were performed to equilibrate systems' periodic boundary condition. Finally, 150ns MD simulation was performed in the NPT ensemble (310K and 1atm). Temperature here was controlled using *Langevin dynamics*[10] and pressure was controlled with the *anisotropic Monte Carlo barostat* in *AMBER14*[11]. All MD trajectories analyses were performed using *cpptraj*[12] as implemented in *AMBER14*[11], the root mean square deviation of the systems and the extraction of representative structures from trajectories. Visualization of the structures was performed with *PyMOL*[9].

Results and Discussion

Agonistic Binding Mechanism of Vilazodone and Its Analogues Identified by MD Simulation

*Ligand **29*** (as shown in **Figure 6A**)

As mentioned in the main text, ligand **29** possessed the highest affinity for receptor with IC_{50} value of 0.30 nM. Besides of the main interaction known to be important for receptor affinity, the extracellular loop 2 and 4 were also involved in the binding process, like $K101^{ECL1}$, $W102^{ECL1}$ and $C187^{ECL2}$. Among them, $K101^{ECL1}$ and $W102^{ECL1}$ interacted with the bicyclic arylpiperazine part via hydrophobic interaction, whereas $C187^{ECL2}$ formed a polar interaction with amide of this part. Around arylpiperazine, hydrophobic interaction could also be detected by several residues ($M92^{2.60}$, $A93^{2.61}$ and $Y96^{2.64}$). It was not surprising that phenyl ring of $Y96^{2.64}$ preferentially directed an almost coplanar orientation (83°-89°) with bicyclic arylpiperazine, which appeared to be a face-to-face π stacking interaction. Similar to $C187^{ECL2}$, $C109^{3.25}$ made polar interaction with the amide. With respect to the distal heterocyclic ring, the residues ($T196^{5.39}$ and $T200^{5.43}$) with 2 polar side chains were essential for stabilizing the nitrile of indole ring via polar interaction. 3 residues ($W358^{6.48}$, $F361^{6.51}$ and $F362^{6.52}$) composed the hydrophobic site, accommodating the hydrophobic molecular fragment of heterocyclic ring.

*Ligand **36*** (as shown in **Figure 6B**)

The absence of bulky bicyclic arylpiperazine part coupled with the presence of monocyclic arylpiperazine

part with small fluorine substituted led to changes of binding mode. Hydrogen bond between heterocyclic ring of these vilazodone analogues and C120$^{3.36}$ was observed, while such interaction of T121$^{3.37}$ in other complexes disappeared. Similarly, the subtle shift of indole resulted in absence of hydrophobic interaction with W358$^{6.48}$. Due to small volume of monocyclic arylpiperazine, it could hardly make interaction with other residues (like K101^{ECL1}, W102^{ECL1}, C109$^{3.25}$ and C187^{ECL2}). F112$^{3.28}$ made edge-to-face π stacking interaction with the aromatic ring substituted by strong electronegative fluorine. T188^{ECL2} resided by D116$^{3.32}$ could stabilize the positively charged nitrogen. Based on the energy contribution, this interaction seemed to compensate the absence of interaction with N386$^{7.39}$.

*Ligand **51*** (as shown in **Figure 6C**)

The affinity of ligand **51** was equivalent to that of **36**, with IC_{50} value of 2.0 nM. The absence of the amide group also reduced the affinity for the receptor in a less degree. The bicyclic arylpiperazine of this ligand could be stabilized by hydrophobic residues (M92$^{2.60}$, A93$^{2.61}$, Y96$^{2.64}$ and W102^{ECL1}). Y195$^{5.38}$ in the vicinity of T196$^{5.39}$ and S199$^{5.42}$ constituted polar binding pocket for nitrile in the indole ring, thus stabilizing the ligand in its binding site.

*Ligand **14*** (as shown in **Figure 6D**)

The affinity of ligand **14** was less than that of **51** with IC_{50} value of 5.0 nM. The removal of nitrile in the heterocyclic ring coupled with the presence of fluorine obviously led to the absence of hydrogen bond with S199$^{5.42}$ and Y195$^{5.38}$ due to the small volume of fluorine. This explained the less affinity of ligand **14** than that of ligand **29**.

*Ligand **39*** (as shown in **Figure 6E**)

The affinity of ligand **39** was less than that of **14** with IC_{50} value of 14.0 nM. Compared with the structure of **36**, 2 substituents (-CN and -OCH_3) were introduced into the phenyl ring of monocyclic arylpiperazine, thus occupied the approximately similar spatial space as that part of **29**. As shown in **Figure 6C**, residues around the monocyclic arylpiperazine included M92$^{2.60}$, A93$^{2.61}$, Y96$^{2.64}$, W102^{ECL1}, C109$^{3.25}$ and I113$^{3.29}$. It was noticeable that F112$^{3.28}$ interacted with ligand by CH-π interaction due to the introduction of OCH_3. Moreover, the structural variation led to reduction of interactions between heterocyclic ring and receptor. The absence of interaction between ligand **39** and receptor residues (T196$^{5.39}$ and T200$^{5.43}$) could explain its low binding affinity to 5-HT_{1A} receptor.

*Ligand **48*** (as shown in **Figure 6F**)

The affinity (IC_{50}) of ligand **48** equaled to 60.0 nM. Compared to structure of **39**, substitution of the nitrile in monocyclic arylpiperazine with electron-donating group -OCH_3 enhanced the electron density, thus leading to a decrease of interaction between monocyclic arylpiperazine and 5-HT_{1A} receptor. Apart from the common binding feature, it was clear that 2 residues (W102^{ECL1} and I189^{ECL2}) was able to stabilize the

phenyl ring of monocyclic arylpiperazine via hydrophobic interaction. The interaction with N386$^{7.39}$ was also absent, which could be responsible for its less affinity than other ligands. As for the heterocyclic ring of ligand **48**, 3 residues (T196$^{5.39}$, T200$^{5.43}$ and A365$^{6.55}$) were involved in the interaction with this moiety similar to that of others. I189^{ECL2} and S190^{ECL2} might compensate the loss of binding energy resulted from the absence of interaction with several residues (like M92$^{2.60}$, A93$^{2.61}$, Y96$^{2.64}$, N386$^{7.39}$), so that ligand **48** still displayed certain binding affinity to 5-HT_{1A} receptor.

The common agonistic binding mechanism shared by vilazodone and all its analogues together with their individual binding characteristics could help medicinal chemists to conduct the rational design of SPARIs for the treatment of MDD. This class of drugs had 2 key structural moieties. One was the arylpiperazine, the positively charged center of which could form salt bridge with D116$^{3.32}$. The other was the indole ring moiety, which could form hydrogen bond with T121$^{3.37}$. Moreover, the linker joined these two parts with certain level of flexibility. Meanwhile, those key residues (M92$^{2.60}$, A93$^{2.61}$, Y96$^{2.64}$, W102^{ECL1}, F112$^{3.28}$ and I189^{ECL2}) identified in this study could stabilize the arylpiperazine part of ligands in 5-HT_{1A} receptor, other key residues (V117$^{3.33}$, C120$^{3.36}$, T121$^{3.37}$, S199$^{5.42}$, A303, F361$^{6.51}$, F362$^{6.52}$, N386$^{7.39}$ and Y390$^{7.43}$) were discovered as favorable for ligands' binding via the heterocyclic moieties.

Supplementary Tables

Table S1. 3-{4-[4-(2, 3-dihydrobenzo[1, 4]dioxin-6-yl)-piperazin-1-yl]butyl}-1H-indol-5-yl derivatives with various substituents on position 5 together with their structures and activities (IC_{50}[a] is in nM).

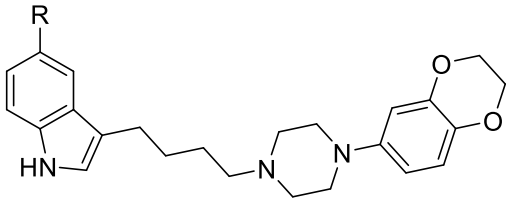

Ligands	R	5-HT_{1A}	RUI[b]	D_2
11	H	8.0±4.0	10.0±11.0	>100
12	OH	0.2±0.15	0.5±0.3	77±36
13	OCH_3	0.5±0.2	100±29	120±35
14	F	5.0±2.3	1.0[c]±0.3	130±61
15	Cl	40.0±17.0	20.0±21.0	>100
16	CHO	0.7±0.4	1.0±0.6	<100
17	C=N-OH	0.4±0.2	5.0±2.0	9.4±4.9
18	COOH	4.0±3.0	N.D.	>100
19	$COOCH_3$	0.6±0.3	50±23	<100
20	$CONH_2$	0.2±0.2	60±22	40±17
21	CN	1.0±0.7	0.4[d]±0.3	5.6±0.6

[a] IC_{50} values were defined as the concentration (nM) leading to 50% of the most inhibition of binding and determined from 5-10 concentrations of compounds, each in triplicate.

[b] PCA: 0.30 mg/kg po; 13% antagonist, 210 min.

[c] PCA: 0.30 mg/kg po; 10% antagonist, 210 min. ED_{50} = 0.44 mg/kg, 210 min, po.

[d] indicates the serotonin reuptake inhibition.

Table S2. The structures and biological activities of 5-F and 5-CN indole derivatives (IC_{50}[a] is in nM).

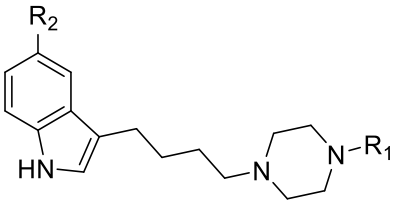

Ligands	R_1	R_2	5-HT_{1A}	RUI[b]	D_2
22	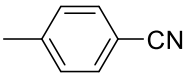	F	40.0±15.0	2.0±0.6	>100
23		CN	1.1±0.2	1.3±0.9	255±45
24	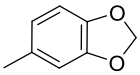	F	4.0±2.0	1.0±0.5	<100
25		CN	0.7±0.4	0.6±0.06	4.9±1.2
26	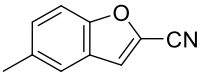	F	5.0±2.0	3.0±1	>100
27		CN	0.4±0.3	1.0±0.7	>630
28	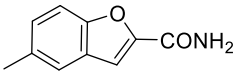	F	3.0±0.9	0.3[c]±0.2	>100
29		CN	0.3±0.06	0.5±0.4	666±75
30	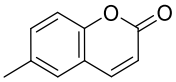	F	0.7±0.2	0.9±0.3	>100
31		CN	0.1±0.06	0.7±0.5	740±232

[a] IC_{50} values were defined as the concentration (nM) leading to 50% of the most inhibition of binding and determined from 5-10 concentrations of compounds, each in triplicate.

[b] RUI indicates the serotonin reuptake inhibition.

[c] PCA: ED50 = 3.80 mg/kg, 210 min, po.

Table S3. The structures and biological activities of 5-CN indole derivatives with different arylpiperazine fragments (IC_{50}[a] is in nM, N.D. refers to not determined).

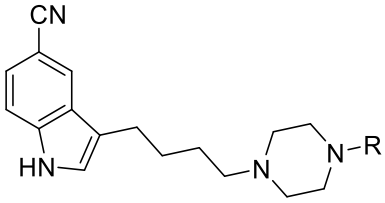

Ligands	R	5-HT_{1A}	RUI[b]	D_2
32	C_6H_5	400±250	1.0±0.7	3.8±2.1
33	4-OHC_6H_4	6.0±2.0	0.5±0.2	35±3
34	4-$OCH_3C_6H_4$	1.0±1.0	0.5±0.4	46±9
35	2- $OCH_3C_6H_4$	1.0±0.2	3.0±0.1	0.7±0.5
36	4-FC_6H_5	2.0±0.6	1.0±0.5	4.2±1.9
37	3, 4-$(CN)_2C_6H_3$	12±7	2.0±0.6	N.D.
38	4-CN-3-$OCH_3C_6H_3$	40±18	2.0±0.9	<100
39	4-CN-2-$OCH_3C_6H_3$	14±14	3.4±0.9	N.D.
40	4-CN-2-$OCH_3C_6H_3$	8.0±0.6	4.1±1.7	6.0±2.9
41	2-CN-3-$OCH_3C_6H_3$	5.6±1.7	3.9±1.1	1.4±0.3
42	2-CN-3-$(OCH_2CH_2)_2OCH_2CH_3C_6H_3$	2.0±0.6	3.2±1.3	28±6
43	3-CN-4-OHC_6H_3	400±200	0.8±0.1	43±21
44	5-Cl-2-$OCH_3C_6H_3$	30±12	6.8±3.4	N.D.
45	3-CN-3, 5-$F_2C_6H_2$	36±18	5.4±1.8	N.D.
46	4-$CONH_2C_6H_4$	118±75	0.6±0.3	>270
47	2-$CONH_2C_6H_4$	6.4±0.7	16±6	47±20
48	3, 4-$(OCH_3)_2C_6H_3$	60±32	0.3±0.1	40±18

[a] IC_{50} values were defined as the concentration (nM) leading to 50% of the most inhibition of binding and determined from 5-10 concentrations of compounds, each in triplicate.

[b] RUI indicates the serotonin reuptake inhibition.

Table S4. The structures and activities of 5-CN indolyl derivatives with the heterobicyclic arylpiperazine substitution (IC_{50}[a] is in nM, N.D. refers to not determined).

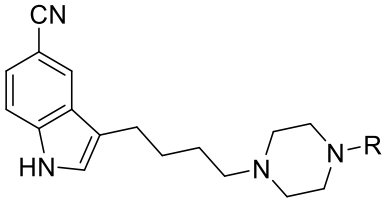

Ligands	R	5-HT_{1A}	RUI[b]	D_2
49		5.0±2.3	0.9±0.6	<42
50		4.0±2.0	1.0±0.6	13±3
51		2.0±1.5	3.1±1.1	31±12
52		1.0±0.4	1.5±0.9	1.4±1.0
53		1.6±0.3	2.4±0.7	5.7±2.7
54		8.7±0.9	3.9±0.8	8.0±4.0
55	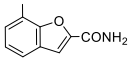	1.9±0.7	2.6±0.9	39±25
56	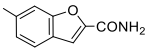	4.4±2.3	1.1±0.5	95±27
57	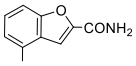	1.4±0.2	8.5±6.0	6.6±2.5
58	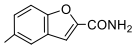	3.2±0.4	3.1±1.2	1400
59	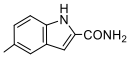	14.0±8.0	2.0±1.4	140±47
60	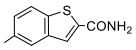	3.1±2.8	0.3±0.1	N.D.
61		3.3±1.3	5.5±2.6	220±99

[a] IC_{50} values were defined as the concentration (nM) leading to 50% of the most inhibition of binding and determined from 5-10 concentrations of compounds, each in triplicate.

[b] RUI indicates the serotonin reuptake inhibition.

Table S5. Binding energy (ΔG_{bind}) calculated from post docking via Prime/MM-GBSA and experimental binding energy (ΔG_{exp}) determined from IC_{50} (ΔG is in kcal/mol and IC_{50} is in nM).

Ligands	IC_{50} [a]	ΔG_{exp} [b]	ΔG_{bind} [c]	Ligands	IC_{50} [a]	ΔG_{exp} [b]	ΔG_{bind} [c]
11	8.0	-11.1	-66.9	37	12.0	-10.8	-60.6
12	0.2	-13.2	-73.7	38	40.0	-10.1	-54.3
13	0.5	-12.7	-72.7	39	14.0	-10.7	-60.6
14	5.0	-11.3	-65.2	40	8.0	-11.1	-66.4
15	40.0	-10.1	-53.4	41	5.6	-11.3	-68.3
16	0.7	-12.5	-71.5	42	2.0	-11.9	-68.9
17	0.4	-12.8	-67.0	43	400.0	-8.7	-47.4
18	4.0	-11.5	-50.4	44	30.0	-10.3	-53.1
19	0.6	-12.6	-72.6	45	36.0	-10.2	-53.1
20	0.2	-13.2	-75.4	46	118.0	-9.5	-49.4
21	1.0	-12.3	-73.8	47	6.4	-11.2	-67.3
22	40.0	-10.1	-53.4	48	60.0	-9.9	-53.7
23	1.1	-12.2	-70.5	49	5.0	-11.3	-69.8
24	4.0	-11.5	-64.8	50	4.0	-11.5	-66.8
25	0.7	-12.5	-71.0	51	2.0	-11.9	-67.1
26	5.0	-11.3	-68.3	52	1.0	-12.3	-70.5
27	0.4	-12.8	-73.0	53	1.6	-12.0	-69.1
28	3.0	-11.6	-63.2	54	8.7	-11.0	-64.3
29	0.3	-13.0	-77.5	55	1.9	-11.9	-67.5
30	0.7	-12.5	-71.5	56	4.4	-11.4	-66.6
31	0.1	-13.6	-78.4	57	1.4	-12.1	-69.7
32	400.0	-8.7	-46.7	58	3.2	-11.6	-67.9
33	6.0	-11.2	-67.8	59	14.0	-10.7	-59.8
34	1.0	-12.3	-70.1	60	3.1	-11.6	-66.6
35	1.0	-12.3	-70.2	61	3.3	-11.6	-65.5
36	2.0	-11.9	-67.7				

[a] Experimental IC_{50} values were collected from the previous publication[13].

[b] The ΔG_{exp} denoted experimentally determined binding free energy, estimated by $\Delta G_{exp} = RTlnIC_{50}$. based on experimental IC_{50} values.

[c] The ΔG_{bind} indicated the binding free energy values obtained by Prime/MM-GBSA approach.

Table S6. Comparison between the calculated and experimental binding energies throughout 6 complexes (ΔG is in kcal/mol and IC_{50} is in nM).

Ligands	Calculated Value						Experimental Value		
	ΔE_{ele}	ΔE_{vdW}	ΔG_{pol}	ΔG_{nonpol}	$\Delta G_{MM/GBSA}$	$\Delta\Delta G_{calc}$ [a]	ΔG_{exp} [b]	$\Delta\Delta G_{exp}$	IC_{50} [c]
29	-22.92±0.23	-58.41±0.17	26.46±0.20	-7.85±0.01	-62.73±0.17	-11.08	-13.00	-3.14	0.30
36	-33.78±0.15	-55.19±0.13	37.01±0.14	-7.67±0.01	-59.63±0.12	-7.98	-11.87	-2.01	2.00
51	-21.96±0.20	-53.87±0.18	24.76±0.14	-7.04±0.01	-58.10±0.13	-6.45	-11.87	-2.01	2.00
14	-15.01±0.20	-53.88±0.14	18.84±0.20	-7.23±0.01	-57.29±0.14	-5.64	-11.33	-1.47	5.00
39	-17.75±0.15	-54.24±0.14	23.24±0.13	-7.43±0.01	-56.17±0.14	-4.52	-10.72	-0.86	14.00
48	-13.46±0.19	-50.10±0.14	18.56±0.15	-6.65±0.01	-51.65±0.15	0.00	-9.86	0.00	60.00

[a] The $\Delta\Delta G$ denoted the change of binding free energy (ΔG) using ligand **48** as a reference.

[b] Estimated free energy values were computed by $\Delta G_{exp} = RTlnIC_{50}$ based on experimental data IC_{50}.

[c] Experimental IC_{50} values collected from the previous publication[13].

Supplementary Figures

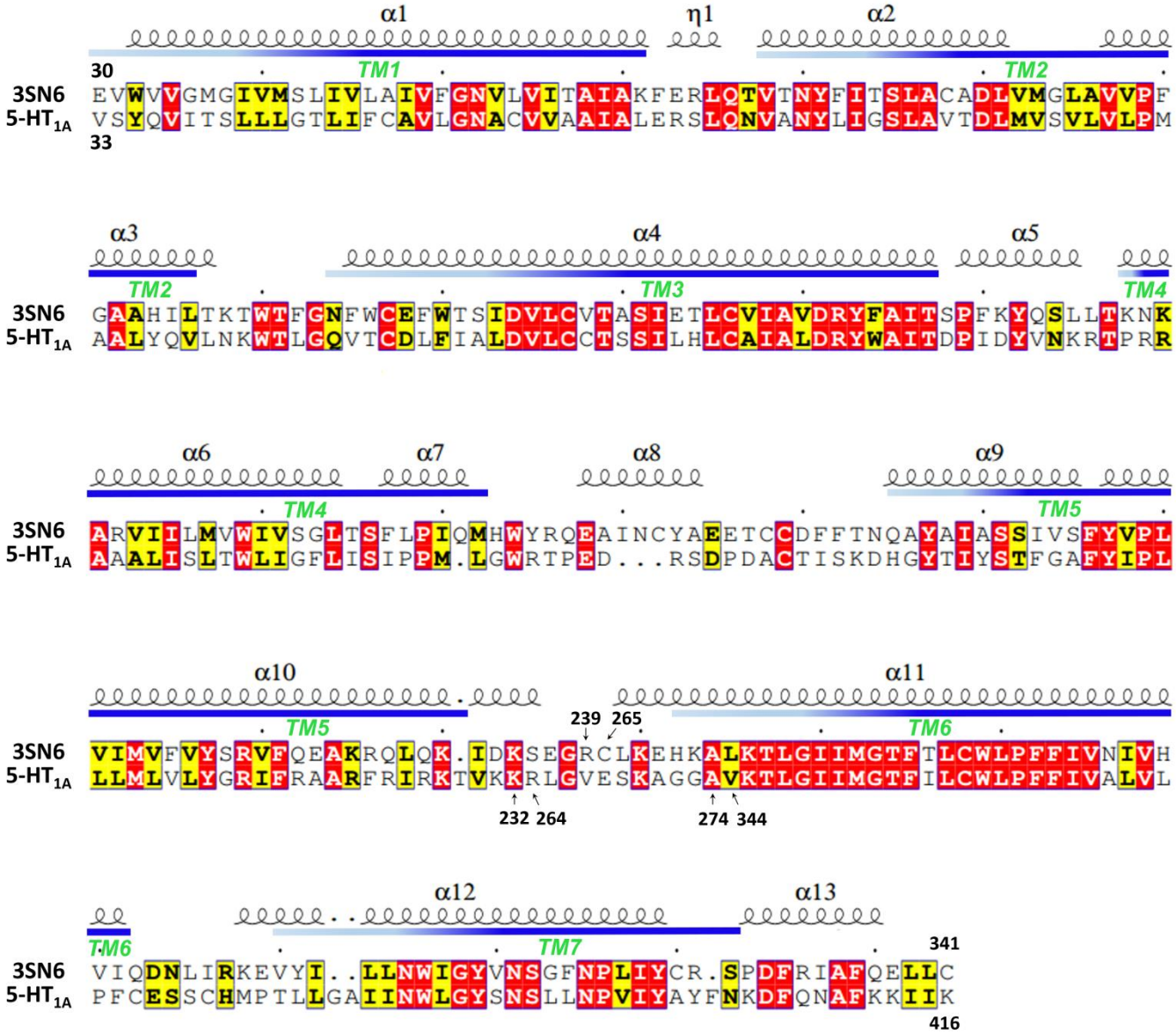

Figure S1. Sequence alignment result between the human 5-HT$_{1A}$ receptor (UniProt Entry: P08909, from V33 to K416) and the template β$_2$AR (PDB entry: 3SN6[14], from E30 to C341). The seven transmembrane (TM1-7) was labeled on sequence, and calculated residue identity between β$_2$AR and 5-HT$_{1A}$ was 34%.

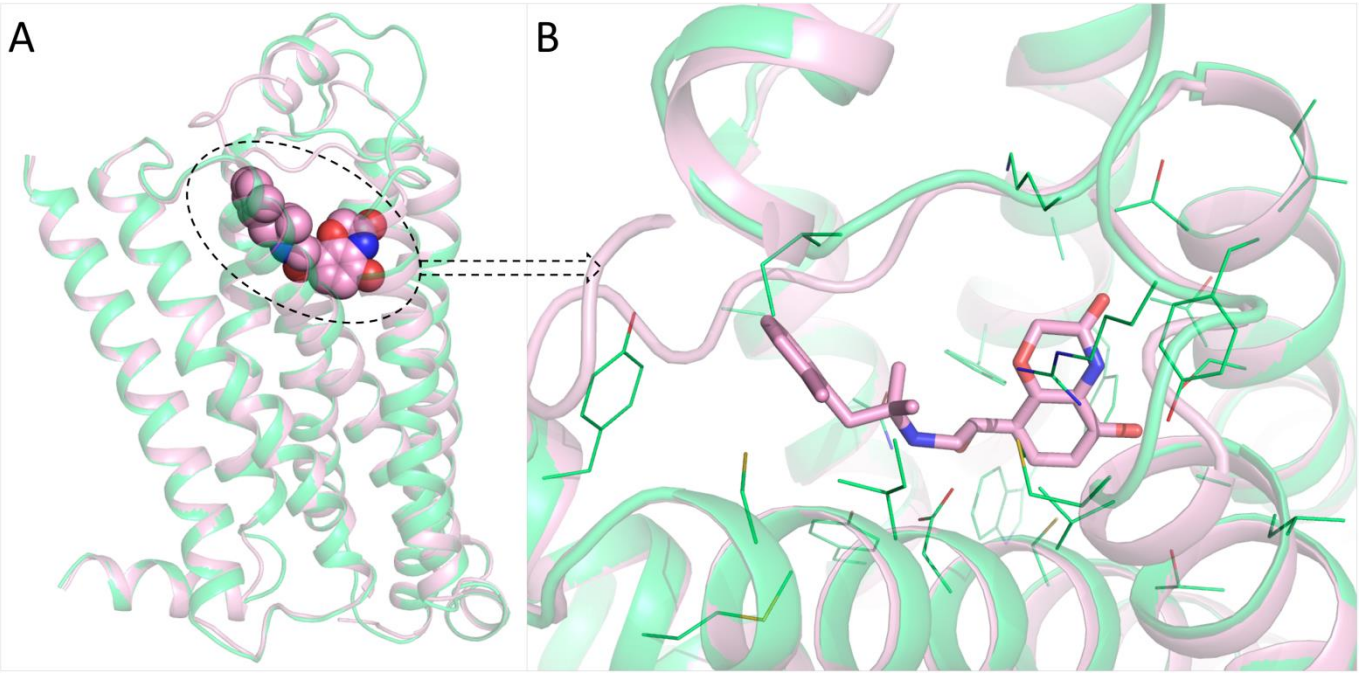

Figure S2. (A) The view of the location of the binding pocket in the 5-HT_{1A} receptor (green) indicated by the location of the crystallized ligand P0G (shown in pink spheres) in the template crystal structure (PDB entry 3SN6[14]) β_2AR (pink). (B) The close view of binding pocket in the 5-HT_{1A} receptor composed by the residues around 6Å distance from crystallized ligand P0G (shown in sticks) in the template and residues displayed in green lines.

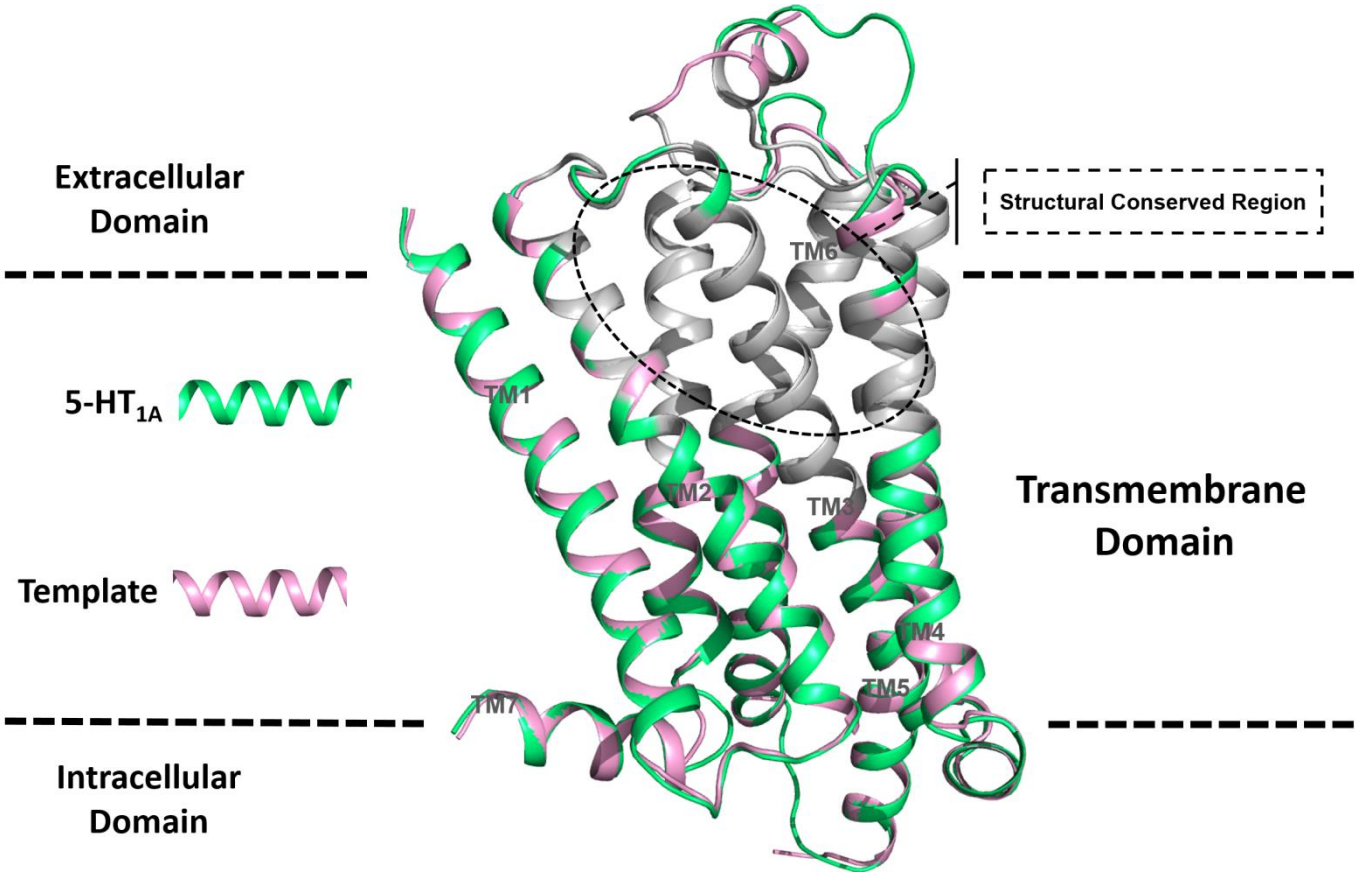

Figure S3. Superimposition of the homology model of 5-HT_{1A} receptor (green) and the template crystal structure (PDB entry 3SN6[14]) β_2AR (pink). The region surrounded by grey ribbons indicated the structural conserved binding pocket for both receptors.

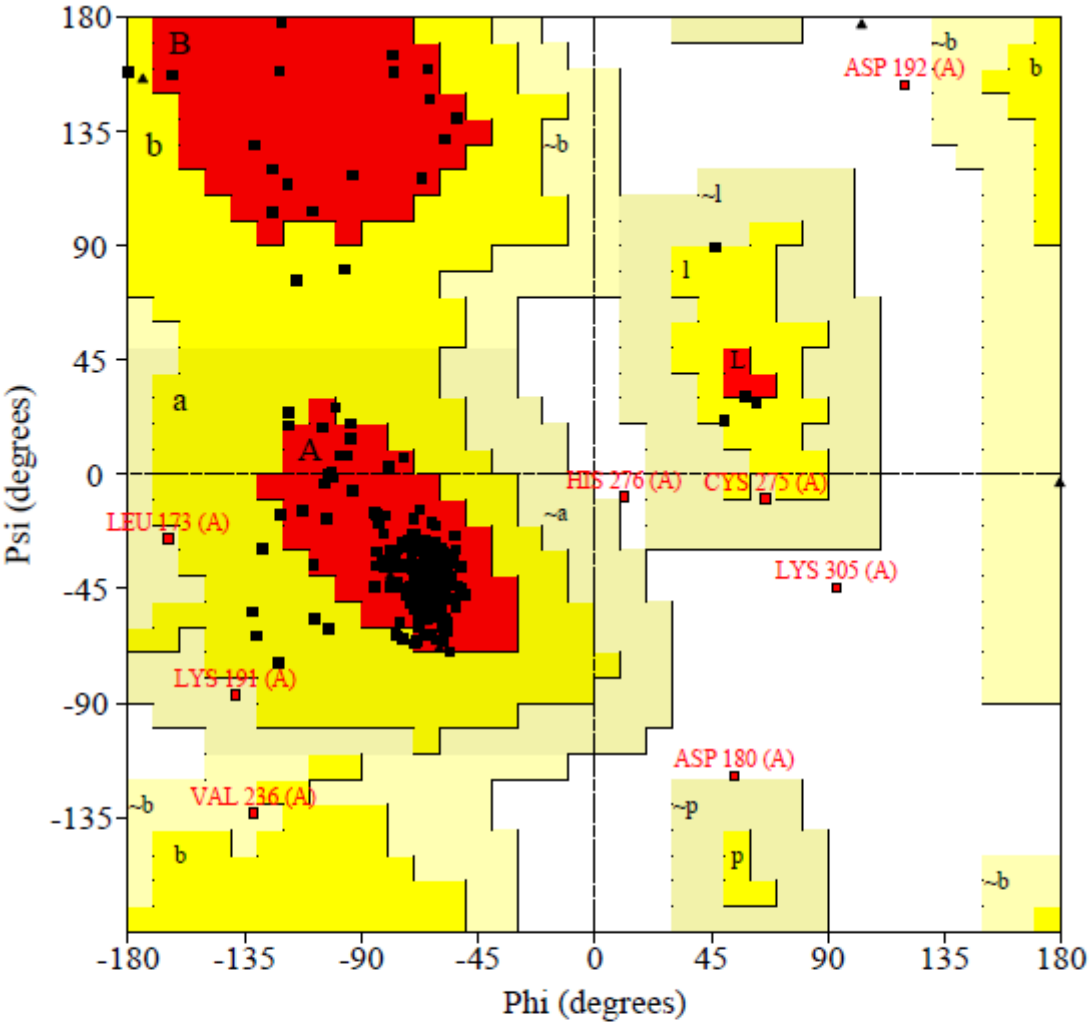

Plot statistics

Residues in most favoured regions [A,B,L]	227	89.4%
Residues in additional allowed regions [a,b,l,p]	19	7.5%
Residues in generously allowed regions [~a,~b,~l,~p]	4	1.6%
Residues in disallowed regions	4	1.6%
	---	------
Number of non-glycine and non-proline residues	254	100.0%
Number of end-residues (excl. Gly and Pro)	2	
Number of glycine residues (shown as triangles)	16	
Number of proline residues	12	

Total number of residues	284	

Based on an analysis of 118 structures of resolution of at least 2.0 Angstroms and R-factor no greater than 20%, a good quality model would be expected to have over 90% in the most favoured regions.

Figure S4. Ramachandran plot of the constructed homology model of the human 5-HT_{1A} receptor.

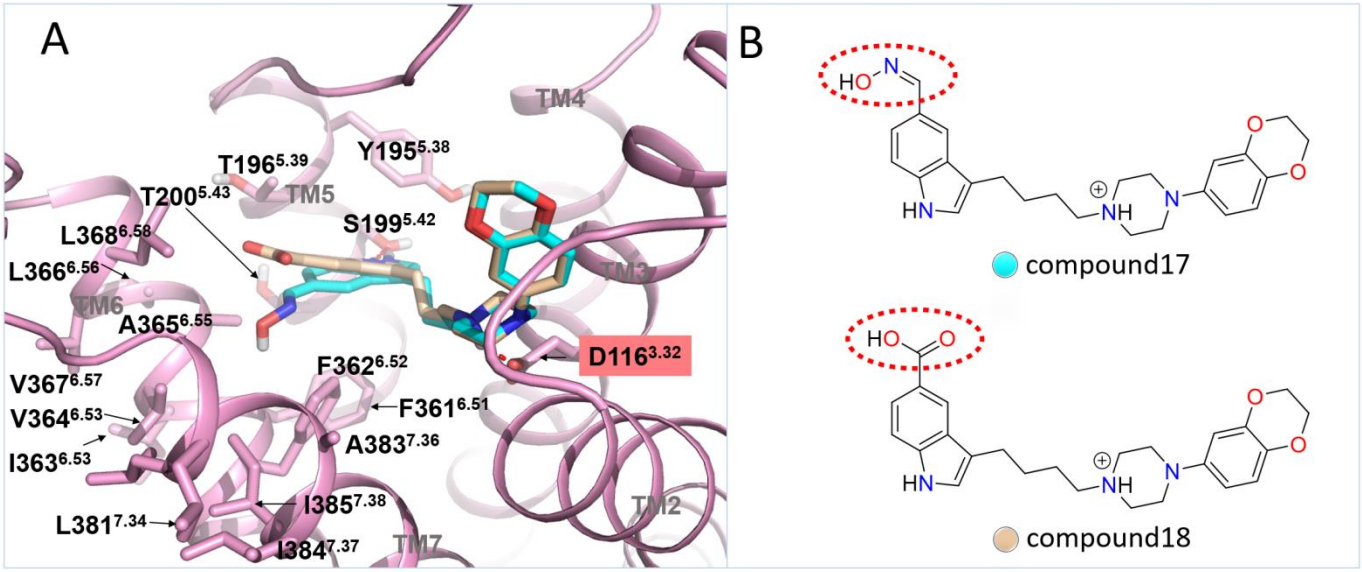

Figure S5. (A) Post processed docking poses of ligand **17** (cyan) and **18** (wheat) in the binding site of the human 5-HT_{1A} receptor (pink). (B) Chemical structures of ligand **17** and **18**. The carboxyl group of ligand **17** and hydroxyimino group of ligand **18** were highlighted in red dashed lines.

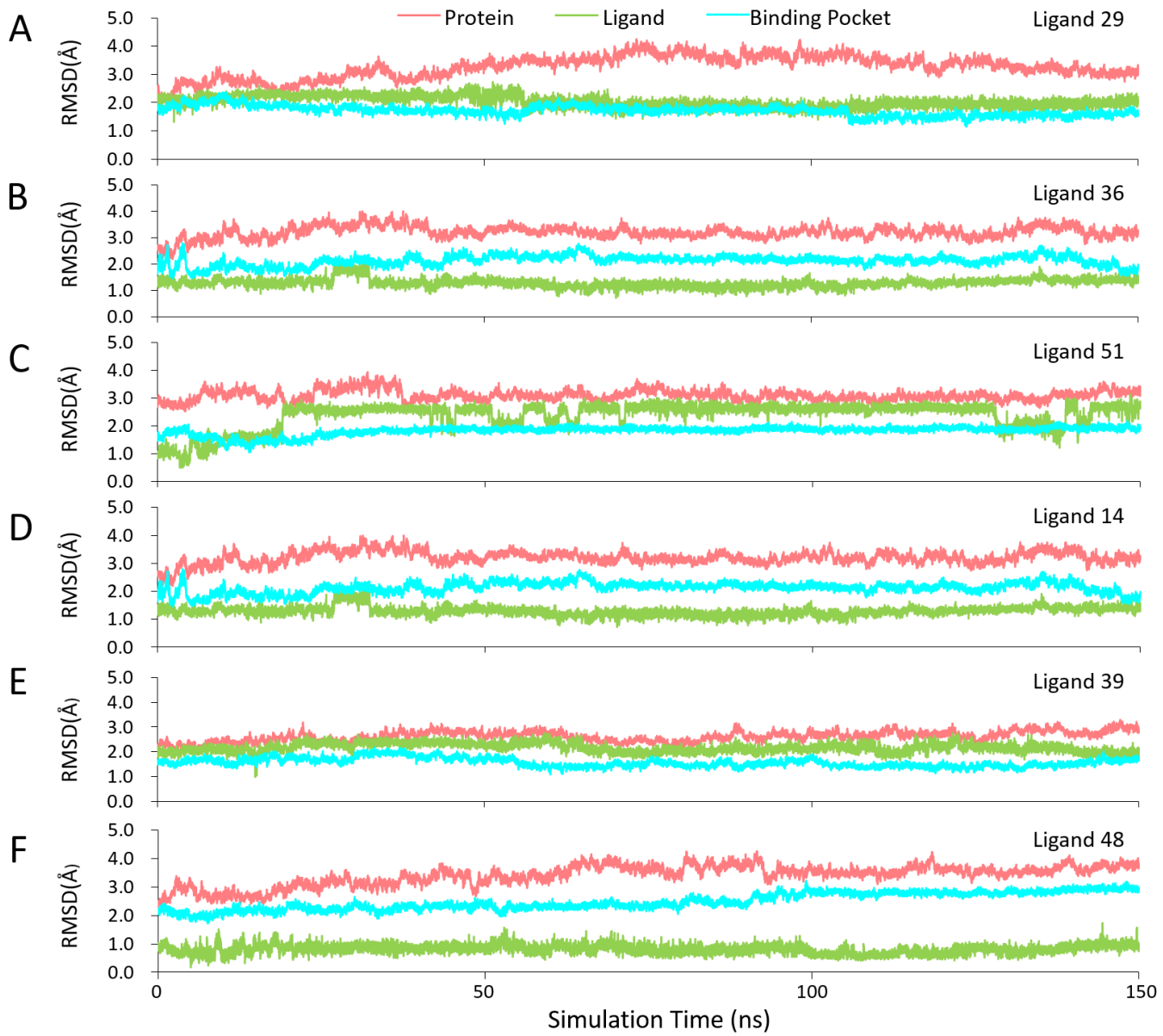

Figure S6. RMSD of protein backbone atoms (red), ligand heavy atoms (green) and binding pocket residue (< 6 Å) backbone atoms (cyan) of the 6 studied complexes against simulation time.

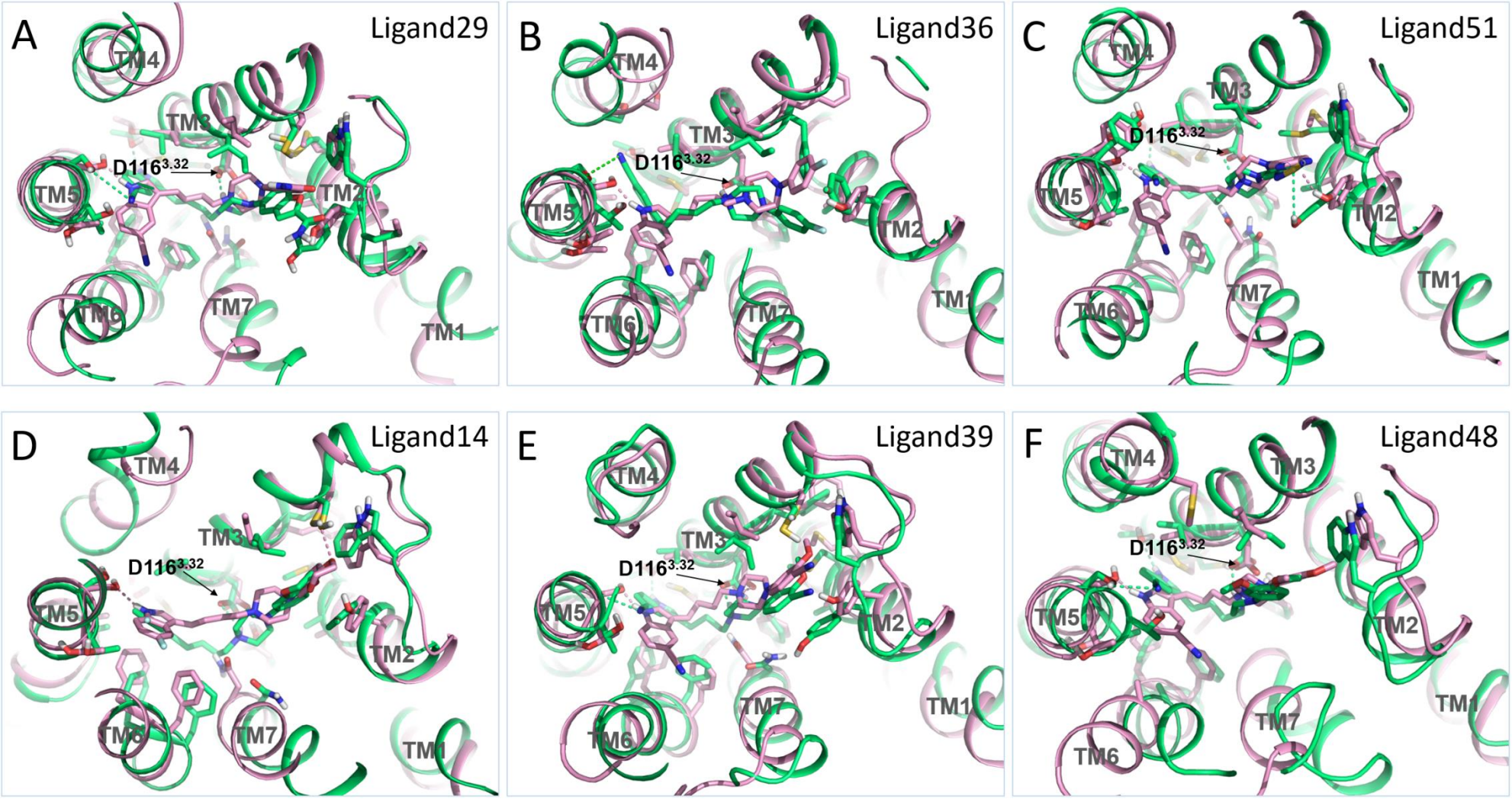

Figure S7. Superimposition of each representative snapshot (green) and initial docking pose (pink). A salt bridge between the positively charged nitrogen of each compound and the carboxyl of D116$^{3.32}$ are constrained and maintained.

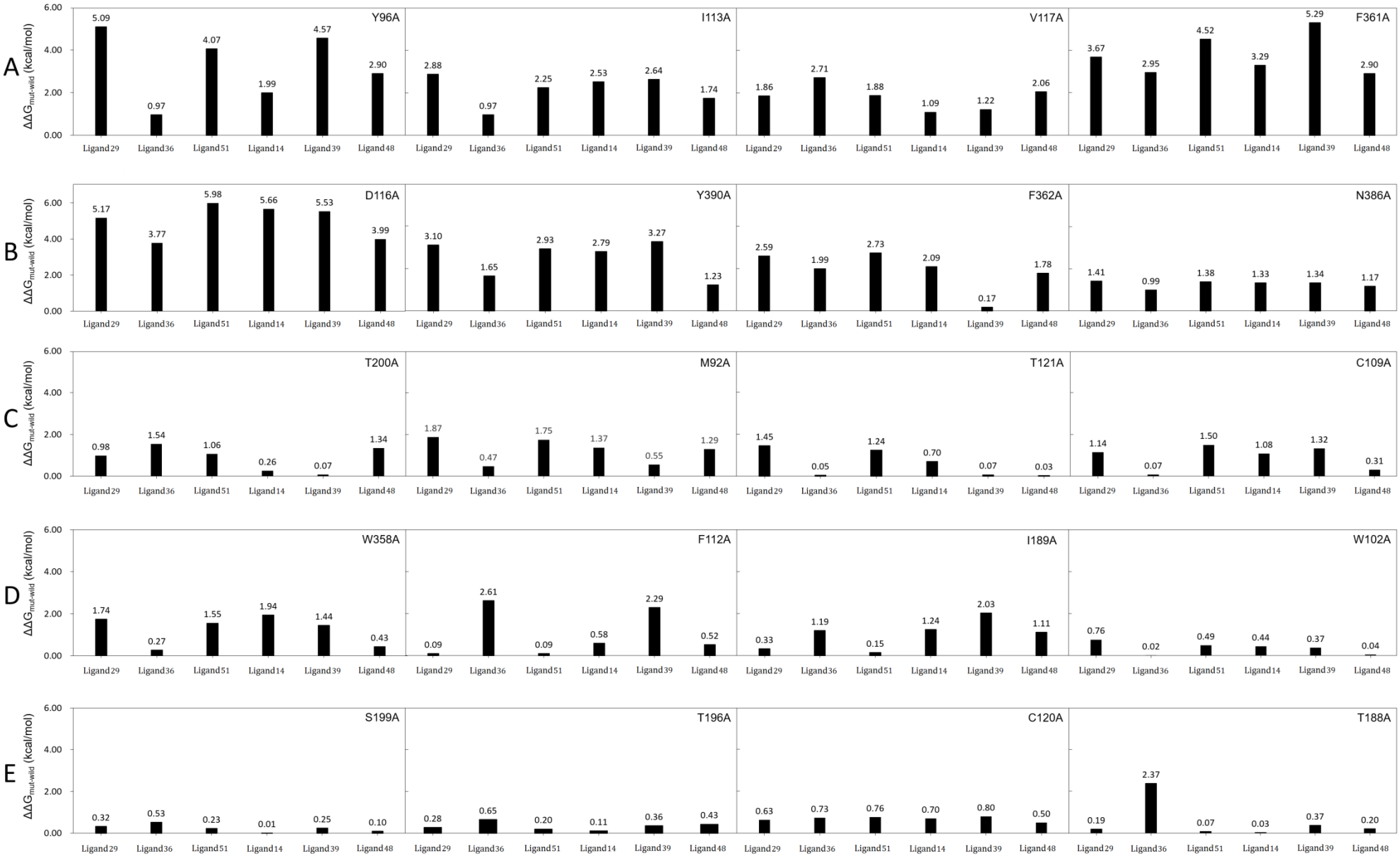

Figure S8. The energy changes ($\Delta\Delta G_{mut-wild}$) of alanine scanning mutagenesis of the key residues identified for 6 studied complexes. (A-E) showed the 5 groups of the energy variances on the basis of the extent of changes.

References

1 Larkin, M. A. *et al.* Clustal W and Clustal X version 2.0. *Bioinformatics* **23**, 2947-2948 (2007).

2 Robert, X. & Gouet, P. Deciphering key features in protein structures with the new ENDscript server. *Nucleic Acids Res.* **42**, W320-324 (2014).

3 Arnold, K., Bordoli, L., Kopp, J. & Schwede, T. The SWISS-MODEL workspace: a web-based environment for protein structure homology modelling. *Bioinformatics* **22**, 195-201 (2006).

4 Lee, J., Lee, D., Park, H., Coutsias, E. A. & Seok, C. Protein loop modeling by using fragment assembly and analytical loop closure. *Proteins* **78**, 3428-3436 (2010).

5 Lee, H., Baek, M., Lee, G. R., Park, S. & Seok, C. Template-based modeling and ab initio refinement of protein oligomer structures using GALAXY in CAPRI round 30. *Proteins* **85**, 399-407 (2017).

6 Lian, P., Li, L., Geng, C., Zhen, X. & Fu, W. Higher-affinity agonists of 5-HT_{1A}R discovered through tuning the binding-site flexibility. *J. Chem. Inf. Model.* **55**, 1616-1627 (2015).

7 Xu, L. *et al.* Molecular modeling of the 3D structure of 5-HT(1A)R: discovery of novel 5-HT(1A)R agonists via dynamic pharmacophore-based virtual screening. *J. Chem. Inf. Model.* **53**, 3202-3211 (2013).

8 Glide, version 5.5, Schrödinger, LLC, New York, 2009.

9 The PyMOL Molecular Graphics System, version 1.3, Schrödinger, LLC.

10 Pastor, R. W., Brooks, B. R. & Szabo, A. An analysis of the accuracy of Langevin and molecular dynamics algorithms. *Mol. Phys.* **65**, 1409-1419 (2006).

11 AMBER 14, University of California, San Francisco, 2014.

12 Roe, D. R. & Cheatham, T. E., 3rd. PTRAJ and CPPTRAJ: software for processing and analysis of molecular dynamics trajectory data. *J. Chem. Theory Comput.* **9**, 3084-3095 (2013).

13 Heinrich, T. *et al.* Synthesis and structure-activity relationship in a class of indolebutylpiperazines as dual 5-HT_{1A} receptor agonists and serotonin reuptake inhibitors. *J. Med. Chem.* **47**, 4684-4692 (2004).

14 Rasmussen, S. G. *et al.* Crystal structure of the beta2 adrenergic receptor-Gs protein complex. *Nature* **477**, 549-555 (2011).